BBA - Bioenergetics 1860 (2019) 533–540

Contents lists available at ScienceDirect

BBA - Bioenergetics

journal homepage: www.elsevier.com/locate/bbabio

Ammonia as a substrate-water analogue in photosynthetic water oxidation: Influence on activation barrier of the O_2-formation step

Ricardo Assunção, Ivelina Zaharieva, Holger Dau*

Freie Universität Berlin, Department of Physics, 14195 Berlin, Germany

ARTICLE INFO

Keywords:
Activation energy
Manganese complex
Oxygen evolution
Oxygen polarography
Photosystem II

ABSTRACT

Information on binding and rearrangement of pivotal water molecules could support understanding of light-driven water oxidation at the catalytic Mn_4CaO_5 cluster of photosystem II (PSII). To address this point, the binding of ammonia (NH_3)—a possible substrate-water analogue—has been investigated and discussed in the context of putative reaction mechanisms. By time-resolved detection of O_2 formation after light-flash excitation, we discriminate three NH_3/NH_4^+ binding sites jointly characterized by a K_m value around 25 mM (of NH_4^+), but differing in their influence on the O_2-formation step. At 100 mM NH_4Cl (pH 7.5), we observe (1) a PSII fraction with complete inhibition of O_2-formation, (2) fast O_2-formation with a time constant of 1.7 ms at 20 °C (Fast-PSII), and (3) slow O_2-formation with a time constant of 36 ms at 20 °C (Slow-PSII). For the Fast-PSII, we determine an activation enthalpy of 223 ± 11 meV. Activation enthalpy and entropy of the Fast-PSII are essentially identical to the corresponding figures in the absence NH_3/NH_4^+ binding. For the Slow-PSII, the activation enthalpy is 323 ± 11 meV and thus significantly increased, whereas the activation entropy remains essentially unchanged. We conclude: (1) The fully-inhibitory binding site could relate to bound NH_3 replacing one of the two substrate-water molecules. (2) The Fast-PSII may relate to NH_3/NH_4^+ binding in the S_2-state of PSII followed by unbinding before onset of the O—O bond formation step, but also more intricate mechanisms are not excluded. (3) In the Slow-PSII, NH_3/NH_4^+ binding increases the energetic barrier of the O—O bond formation step significantly.

1. Introduction

In oxygenic photosynthesis, visible light drives a complex series of reactions, including the pivotal oxidation of water [1–3]. As a by-product of the water-oxidation reaction, the atmospheric dioxygen has been produced. Lately, the process has gained increased attention as biological water oxidation serves as bio-inspiration for creating synthetic solutions of water oxidation for renewable solar fuels (see, e.g., [4,5]). In the photosynthetic organisms, the reaction occurs in Photosystem II (PSII), a large protein complex embedded in the thylakoid membranes of plants and cyanobacteria [1–3]. In PSII, the absorption of a photon and rapid excitation energy transfer is followed by electron transfer from chlorophylls (Chl) denoted as P680 to a pheophytin (Pheo) and from there to a protein-bound plastoquinone (Q_A) (Fig. 1A). The final electron acceptor in PSII is a second plastoquinone (Q_B) which, after being reduced twice leaves the PSII and joins the so-called plastoquinone pool; subsequently the Q_B site is refilled by another (not reduced) quinone molecule. The positive hole created on P680 is compensated by hopping of one electron from a specific redox-active tyrosine residue (Yz), which is in turn reduced by an electron from the catalytic site of water oxidation, the oxygen evolving complex (OEC), consisting of a Mn_4CaO_5 metal cluster and its protein environment, also including several mechanistically crucial protein-internal water molecules. Successive absorption of four photons facilitates four successive steps of oxidation of the OEC. Because of interlaced proton removal steps, these oxidation steps are not associated with the accumulation of several positive charges [6–8].

In the classical picture of Kok and coworkers [9], the catalytic OEC cycle involves five oxidation states, the dark stable S_0 and S_1 states, the semi-stable S_2 and S_3 and the transient S_4 state between S_3-S_0 preceding the oxygen release. An extended S-state cycle describes in more detail this sequence of events, including the alternating removal of electrons and protons from the OEC, thereby keeping the redox potential for each electron removal step (by electron transfer to Y_Z) sufficiently constant (Fig. 1B) [10–12]. The structure of the S_1 state of the Mn_4CaO_5 cluster has been resolved by protein crystallography at a 1.95 Å resolution, including the position of neighboring water molecules. Two of these water molecules are directly bound to a manganese ion (Mn4) and two

* Corresponding author.
E-mail address: holger.dau@fu-berlin.de (H. Dau).

https://doi.org/10.1016/j.bbabio.2019.04.005
Received 23 February 2018; Received in revised form 20 December 2018; Accepted 6 January 2019
Available online 26 April 2019
0005-2728/

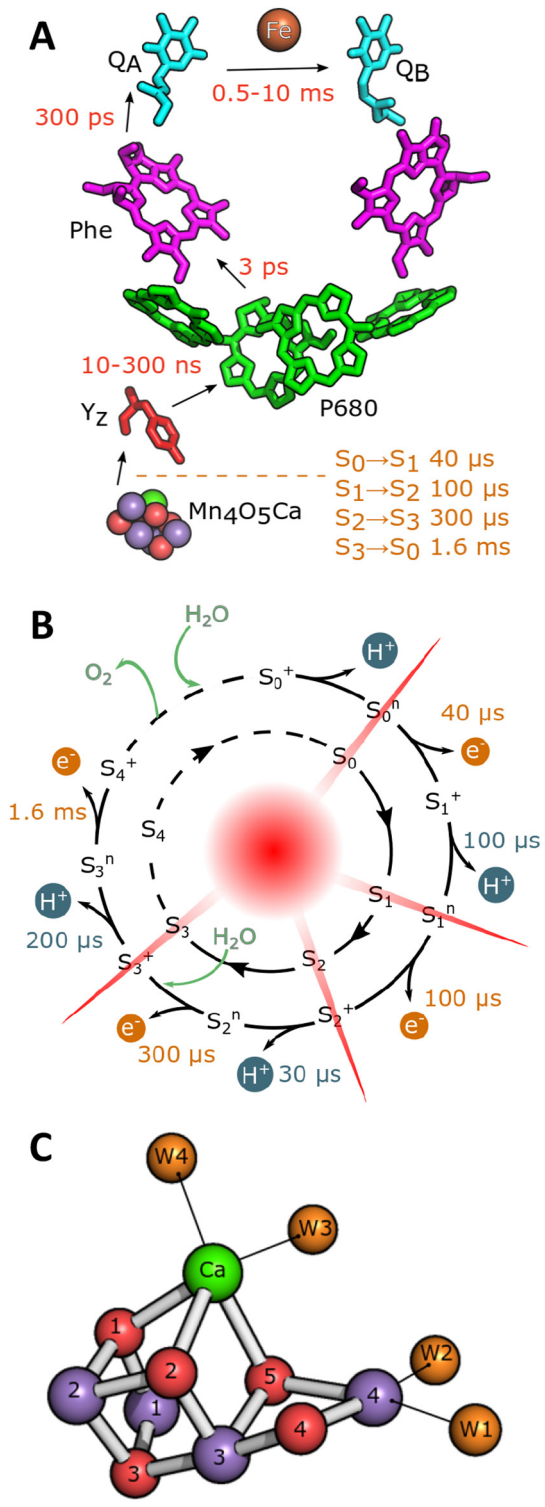

Fig. 1. (A) Important cofactors of photosystem II (PSII): P680 (chlorophylls), Phe (pheophytin), Q_A and Q_B (plastoquinones), non-heme iron(II) ion, Yz (tyrosine 161 of the D1 protein of PSII) and the protein-bound Mn_4CaO_5 cluster. (B) The reaction cycle of PSII water oxidation, with the classical representation in the inner circle and the extended S-State cycle model outside. Red spikes represent light flashes that induce the S-state transitions. In dark-adapted PSII, the S_1-state prevails so that the first flash induces the $S_1 \rightarrow S_2$ transition. The subscripts in the S-state notation indicates the number of accumulated oxidizing equivalents while the superscripts indicate the charge ('n' for neutral and '+' for positively charges). (C) Mn_4CaO_5 cluster in its dark-adapted S_1 state, with four water molecules (H_xO, x = 2, 1, or 0) terminally coordinated to either Mn4 or the Ca ion ($W_{1–4}$). Red spheres represent O atoms, the purple spheres represent Mn atoms, green spheres represent calcium, and the water molecules are shown in orange. Graphical representations in (A) and (C) according to the crystallographic model of Umena et al. [13].

to the calcium ion, as shown in Fig. 1C [13,14]. Efforts in computational chemistry have been directed towards understanding of the S-state transitions at the atomic (and electronic) level, including evaluation of alternative O—O bond formation mechanisms, taking into account both structural and spectroscopic data [15–17]. The two most favored basic options to explain efficient O—O bond formation are (i) nucleophilic attack and (ii) a radical-coupling mechanism. A specific variant of the latter mechanism is especially often invoked in mechanistic discussions; it has been proposed and elaborated by Siegbahn [16,18]. Various variants of the two basic options are still controversially debated [19–23].

Recently, we showed that the (partial) inhibition of PSII oxygen evolution in the presence of NH_4Cl is largely due to an on/off effect of the O_2 activity [24] and cannot be explained exclusively by slowed oxygen evolution [25]. Depending on the NH_4Cl concentration, a fraction of about 50% of the PSII cores were fully inhibited, for spinach as well as cyanobacterial PSII. In the major fraction of the O_2-active PSII, the rate constant of O_2 formation was found to be independent of the ammonium concentration in the buffer solution. To explain the experimental results, we proposed anti-cooperative binding at two sites, either to the inhibitory site or to the non-inhibitory site. The two binding sites were proposed to correspond to the W1 and W2 water molecules coordinated to Mn4, the "dangler manganese" (Fig. 1C), but possibly also involving the carousel mechanism of water and ammonia binding proposed by Brudvig, Batista and coworkers [22,26]. We also found that among the O_2-producing PSII centers, PSII centers with O_2 evolution kinetics unaffected by ammonia binding are coexisting with a fraction of "slow" PSII, which was explained by a third ammonia binding site [24].

In the present work, we use time-resolved O_2 polarography for analysis of the temperature-dependence of ammonia inhibition, with focus on determination of thermal activation energies of O_2 formation in the presence of ammonia. Using Eyring's transition-state treatment [27], we also analyze the thermodynamics parameters of the O_2 evolution reaction in ammonia-treated PSII. Ammonia binding was induced by addition of various concentrations of NH_4Cl to the buffer solution. For a detailed discussion of the relation between NH_4^+ concentration and ammonia binding, see [24].

2. Materials and methods

2.1. Preparation of plant-PSII membrane particles

High-activity PSII-enriched membrane particles were prepared from spinach leaves, as described elsewhere [28]. Before storage at −80 °C, the chlorophyll concentration was determined according to Wellburn [29]. Using a Clark-type electrode (*Hansatech Instruments*) [30], an O_2-evolution activity of 860 ± 20 $\mu mol_{O2}\ mg_{Chl}^{-1}\ h^{-1}$ was determined at 25 °C for the PSII membrane particles illuminated with continuous white light of saturating intensity. The measurements were done in buffer containing 15 mM NaCl, 5 mM $CaCl_2$, 1 M glycine betaine, 25 mM 2-morpholinoethanesulfonic acid (pH 6.3) with additional 0.25 mM 2,6-dichloro-1,4-benzoquinone (DCBQ) and 1 mM $K_3[Fe(CN)_6]$ as artificial electron acceptors [28].

2.2. Time-resolved oxygen polarography

Time-resolved oxygen evolution measurements were performed using a centrifugable custom-made bare platinum electrode as

described earlier [24,31]. Before use, the frozen PSII suspension was thawed on ice (for 60 min, in the dark) and resuspended in Buffer A [150 mM NaCl, 25 mM MES (pKa = 6.15), 25 mM HEPES (pKa = 7.55), 25 mM HEPES (pKa = 8.0), 1 M glycine betaine, 5 mM $MgCl_2$, and 5 mM $CaCl_2$, pH 7.5 (NaOH)]. The protein sample was then centrifuged at 50,000 ×*g* for 12 min, the supernatant discarded, and the resulting pellet resuspended again in Buffer A and kept on ice. For each measurement a sample containing 75 µg chlorophyll and a combination of Buffer A and Buffer B (same as Buffer A with 150 mM NH_4Cl instead of 150 mM NaCl) setting the desired NH_4Cl concentration (0–100 mM Buffer A-B mix) were added to the electrode. Thereby the total chloride concentration was kept constant at the level of 170 mM. Fig. S1 shows that at this salt level the yield and reaction kinetics of O_2 formation was not negatively affected (no inhibition up to 330 mM). The total volume of the PSII suspension over the electrode was adjusted to be 750 µL, followed by centrifugation of the electrode assembly in a swing-out rotor at 10,000 ×*g* for 10 min (at 4 °C).

S-state transitions were excited in the dark-adapted PSII using saturating light flashes of about 10 µs duration (Xenon flash lamp, *EG&G Optoelectronics*, 4.5 J of electrical energy per flash, an orange glass filter with 570 nm cut-off was used to eliminate photoelectric flash artefacts induced by blue light). The individual oxygen-evolution transients were measured with a flash spacing of 900 ms for 20 flashes and an electrode potential of −0.95 V at the central Pt electrode vs the Ag ring electrode; the potential was switched on 15 s prior to the first flash. A home-built potentiostat was used for electrode polarization and detection of the O_2-reduction currents, the latter involving a high-pass filter with a time constant of 100 ms. The high-pass filter separates the light-induced O_2-transients from an approximately linear decrease in the O_2-signal. The latter results from detection and consumption (by the polarized platinum electrode) of dioxygen dissolved in the buffer solution. The simulations in Fig. S2 illustrate how the high-pass filter affects the O_2 signal. Its influence was considered in the fit algorithm used for simulation of the O_2 transients (using a fixed value of the filter time constant of 100 ms). The temperature (0–35 °C) was controlled by Peltier elements and monitored during the measurement by a miniature sensor immersed in the buffer solution of the O_2 flash experiment. The O_2-evolution transients were simulated based on a reaction–diffusion model first described in Dilbeck et al. [31]. This numerical model takes into account the oxygen production from the PSII layer, the O_2 diffusion within the PSII layers (towards electrode surface and into the buffer solution), and the O_2 reduction reaction at the electrode surface using a minimum of adjustable parameters [31]. In addition, the simulations covered two populations of O_2-producing PSII, as introduced in Schuth et al. [24], each with two individual time constants (τ_{lag} and τ_{O2}), but with identical electrode and diffusion parameters (effective layer thickness) for both PSII fractions (Fig. 2A). The total O_2 signal was simulated as a linear combination of the O_2 transients calculated for the two PSII fractions with the percentage of the slow PSII fraction being a fit parameter. In all simulated O_2 transients, also the influence of the high-pass filter was part of the computational model.

2.3. Reversibility of NH_4Cl treatment

For evaluation of the reversibility of NH_4Cl treatment, after thawing the PSII sample was divided into three portions, which were resuspended and centrifuged two times. The first portion was two times resuspended in Buffer A (no NH_4Cl) and the third portion was two times resuspended in a buffer containing 100 mM NH_4Cl (appropriate Buffer A/B mix). The second portion was first centrifuged in 100 mM NH_4Cl (appropriate Buffer A/B mix) and then resuspended and centrifuged in Buffer A (no NH_4Cl). Subsequently each portion was investigated at 15 °C using the O_2 polarography procedure described above, using the buffer of the second resuspension step (first and second portion in Buffer A without NH_4Cl; third portion with 100 mM NH_4Cl).

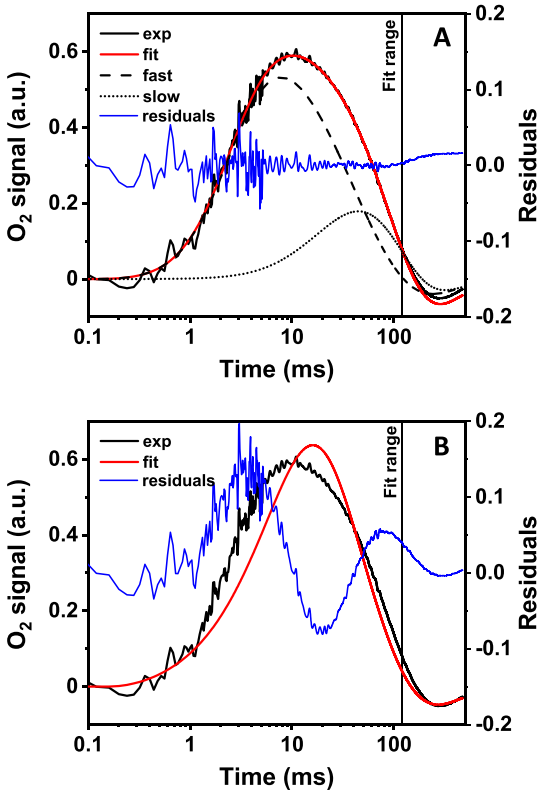

Fig. 2. Example of an experimental O_2 transient (exp) with simulated curves (fit). In A, curve-fitting for two fractions of O_2-producing PSII (Fast-PSII and Slow-PSII). In B, curve-fitting for a single PSII fraction. Only the PSII-layer thickness was kept at the same level in the otherwise fully independent fits in A and B. The shown data was collected at 15 °C in the presence of 100 mM NH_4Cl and the O_2-formation for three reaction cycles of water oxidation by PSII were averaged (12 transients induced by saturating flashes of visible light sequentially applied to the same PSII sample). In A, the time constants of O_2 formation (τ_{ox}) and the relative fractions of PSII with fast and slow oxygen evolution were 2.0 ms (55%) and 46 ms (45%). In (B), only a single fraction was used (100%) and the fit algorithm provided a value of 7.2 ms. In A and B, the negative currents at times exceeding 100 ms resulted from the use of a high-pass filter in the detection electronics (Fig. S2), which was appropriately considered in the numerical simulation of the O_2 transients.

3. Results

To verify the absence of irreversible modifications of PSII by NH_4Cl exposure in the dark, we exposed PSII for 20 min to 100 mM NH_4Cl and then exchanged the buffer against NH_4Cl-free buffer. By exchanging the buffer twice, the O_2 evolution activity was completely restored (Fig. S3). This control experiment shows that also prolonged dark-exposure of PSII to 100 mM NH_4Cl does not result in any specific deleterious effect on O_2-evolution by PSII.

Aiming at the NH_4Cl influence on the thermal activation energy of the water oxidation reaction, we investigated O_2-release kinetics of plant PSII membrane particles (prepared from spinach) by time-resolved O_2 polarography at different temperatures. The time-resolved O_2 detection after excitation of dark-adapted PSII membrane particles by sequences of saturating microsecond flashes of visible light (flashes spaced by 900 ms) allows us to discriminate between the NH_4Cl influence on the rate constant of the O_2 formation step, the efficiency of the S-state transitions, and the fraction of PSII with complete inhibition of the O_2-formation step; the influence of reactions at the PSII acceptor side can be safely ignored [24]. Therefore, analysis of these transients provides a clearly more differentiated picture than obtainable by the conventional detection of the rate of O_2-formation for continuous

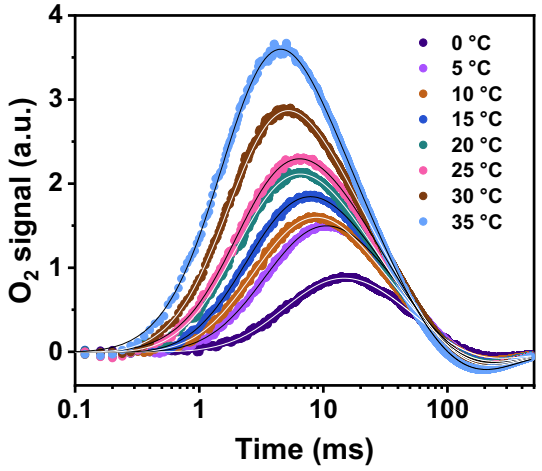

Fig. 3. O_2-evolution transients of PSII membrane particles at various temperatures. The PSII membrane particles were deposited on a bare platinum electrode by joined centrifugation of a PSII solution and the Pt/Ag electrode assembly. Here the temperature dependence of the O_2 transients is shown for PSII membrane particles without NH_4Cl in the buffer system. The white and black lines were obtained by simulations based on a numerical model that takes into account the O_2-formation and diffusion in the PSII layer as well as the O_2 reduction at the bare platinum electrode. The simulation parameters were determined by a fit procedure; the high fit quality is visible when comparing the simulated curves (smooth white and black lines) and experimental transients (colored data points).

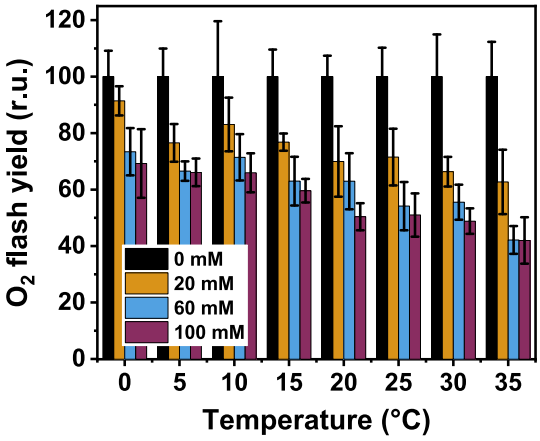

Fig. 4. Influence of NH_4Cl on the O_2-production per saturating light flash. The shown O_2-flash yield provides a relative measure of the total amount of produced dioxygen, independent of the rate constants of O_2-formation step. It corresponds to the integral of the O_2-electrode signal as determined by the simulation approach detailed further below. All measurements were done at pH 7.5. The filled bars indicate the mean value of minimally three repetitions (with averaging of 12 O_2 transients each). The error bars indicate standard deviations, which are predicted to exceed the 1σ-uncertainty range of the mean value.

illumination of PSII in the presence of artificial electron acceptors.

In order to address the activation energy of the O_2-formation step in the presence of bound NH_4^+/NH_3, we measured O_2-release transients at eight temperatures ranging from 0°C to 35 °C. For each temperature, measurements were performed in the presence of 0, 20, 60 and 100 mM NH_4Cl, while keeping the chloride concentration and ionic strength constant by addition of complementary amounts of NaCl. The temperature modified the oxygen evolution traces by affecting both, the electrode response and the rate constants related to water oxidation reaction in PSII. As a result, the total amplitude of the O_2-release signal increases with temperature (Fig. 3), resulting in especially favorable signal-to-noise ratios at higher temperatures. From the O_2 transients, we determined the O_2-forming fraction of PSII at various NH_4Cl concentrations (Fig. 4). At 35 °C, the inhibitory effect of NH_4Cl is especially pronounced (close to 60% inhibition at 100 mM NH_4Cl); at 0 °C it is especially weak (close to 30% inhibition). Its magnitude is in reasonably good agreement with values reported previously for data collection at 10 °C, for oxygen evolution by PSII from spinach and from various cyanobacteria [24]. Noteworthily, there are no indications for a pronounced temperature dependence of the K_m of NH_4^+/NH_3 binding suggesting that the previously determined K_m of about 25 mM [24] could describe the behavior at all investigated temperatures (with a caveat for the 0 °C data, where the seeming lack of inhibition at 20 mM NH_4Cl may be explainable by comparably high noise contributions).

As shown previously [24], NH_4Cl does not only inhibit a major fraction of PSII completely, but it also slows down drastically the O_2-evolution rate constant in another fraction of PSII centers. We simulated the O_2 transients by employing a one-dimensional diffusion model that covers light-induced O_2 production (by PSII), O_2 diffusion (within the PSII film and in the bulk solvent), and O_2 reduction (at the bare Pt electrode), as described elsewhere [24,31]. The slowing down in the decay of the polarographic signal observed with increasing NH_4Cl concentration (Fig. 5A), is well explained by assuming coexistence of two O_2-producing PSII populations: (i) a PSII fraction with fast oxygen evolution (1.7 ms at 20 °C) and (ii) a PSII fraction with slow oxygen evolution (36 ms at 20 °C) [24]. The temperature dependence of the relative contributions of the three PSII fractions at various NH_4Cl concentrations are shown in Fig. 5B–D; the corresponding time constants of the O_2-formation step are shown in the form of Arrhenius plots in Fig. 6; for further simulation parameters, see Fig. S4.

The time constant for O_2 release (τ_{O2}) by PSII in the absence of NH_4Cl is found to be about 1.7 ms at 20 °C. This value agrees well with time constants for PSII oxygen evolution reported before (see, e.g., [32]) and is not modified by the presence of NH_4Cl in the Fast-PSII fraction (Fig. 6A). On the other hand, the O_2 evolution time constant for the Slow-PSII fraction is about 36 ms. This value is similar to the time constants reported for PSII mutants with point mutations at amino acid residues that interact with the water cluster surrounding the Mn_4CaO_5 core of the OEC (e.g. D1-D61, D1-V185, D2-K317 and CP43-R357) [31,33–35]. Similar to the Fast-PSII fraction, at all investigated temperatures the O_2-evolution time constant of the Slow-PSII does not depend on the NH_4Cl concentration (Fig. 6B).

To extract the activation energies (E_a) for the O_2-evolution reaction, the time constants were plotted as function of the temperature (Fig. 6) and fitted using the standard Arrhenius equation:

$$\ln(\tau) = -ln(A) + E_a/K_B T \quad (1)$$

The thereby obtained activation energies (E_a) and the pre-exponential factors (A) are presented in Table 1. We find that the activation energies for both O_2-producing PSII fractions are independent of the NH_4Cl concentration. The activation energy for the Fast-PSII fraction is 248 ± 11 meV and for the Slow-PSII fraction it is 348 ± 14 meV (see Table 1 for the individual values). The plots for the time constants related to the proton-release step (τ_{lag}) preceding the O—O bond formation are shown in Fig. S5. Unlike the O_2 formation step, a slight NH_4Cl dependence may be present, but it is below the uncertainty range of the experimental data and thus not further discussed.

Based on Eyring's transition state theory [27], we determined activation enthalpy, $\Delta H^{\ddagger}$, and activation entropy, $\Delta S^{\ddagger}$, of the O_2-evolution reaction according to Eqs. (2) and (3), respectively (Table 1).

$$\Delta H^{\ddagger} = E_a - k_B T_0 \quad (2)$$

$$\Delta S^{\ddagger} = k_B \ln(hA/k_B T) - k_B \quad (3)$$

In the above equations, k_B is the Boltzmann constant, h is the Planck constant, T refers to the absolute temperature in Kelvin, and T_0 is a

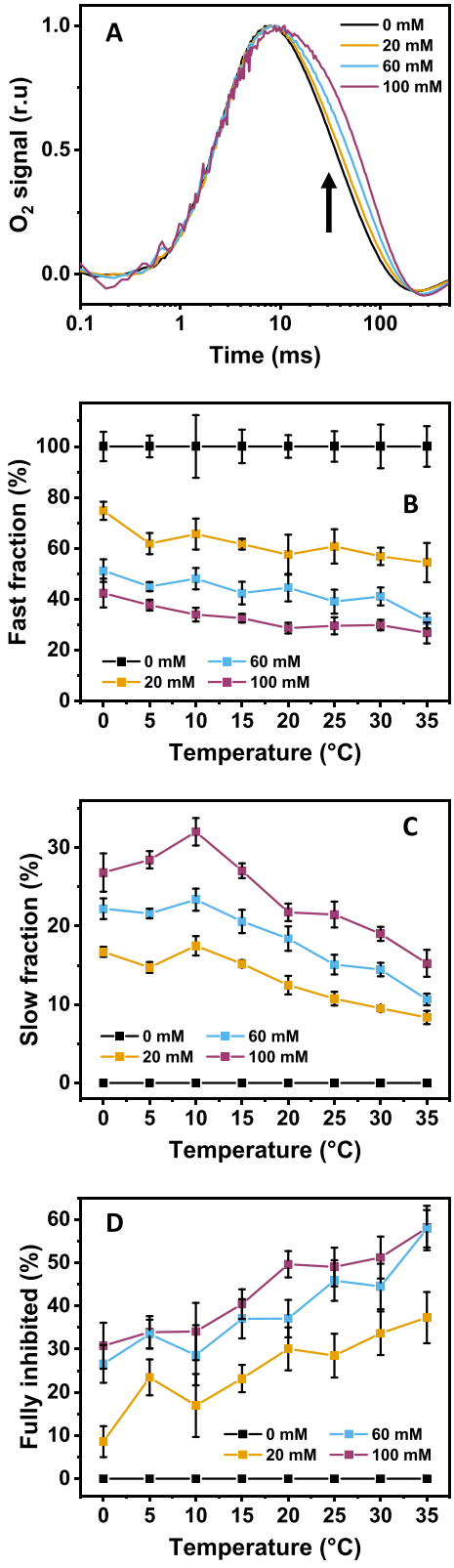

Fig. 5. Relative fractions of PSII centers with fast, slow and fully inhibited O_2-formation. (A) Normalized O_2 release kinetics recorded at 15 °C. The signature of a slow PSII fraction at higher NH_4Cl concentration is indicated by an arrow. (B) Fraction of PSII with fast O_2-formation (1.7 ms at 20 °C). (C) Fraction of PSII with slow O_2-formation (35 ms at 20 °C). (D) Fraction of fully inhibited PSII. The quantification is based on simulation (fit) the O_2-transients with the reaction-diffusion model described elsewhere [24,31]. The simulated O_2-transients were obtained by averaging the O_2-transients detected for the 3rd to 14th flash of a flash sequence applied to dark-adapted PSII. For each data point, the fit results of three experiments were averaged; the error bars indicate the corresponding standard deviation.

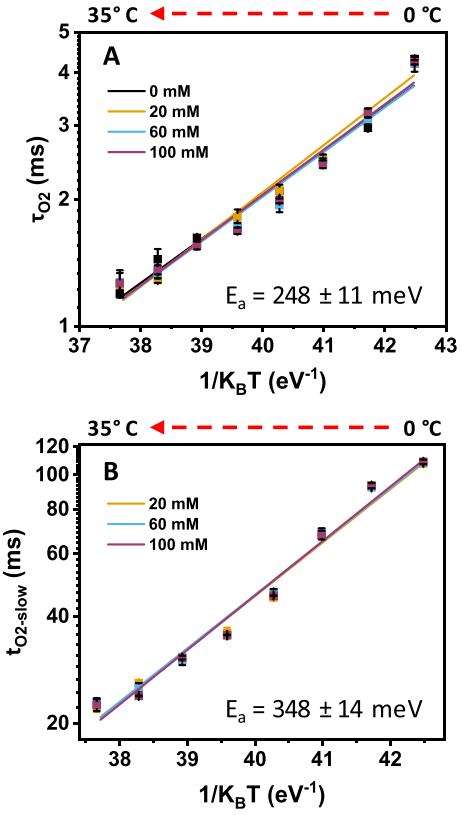

Fig. 6. Arrhenius plots for O_2-release step at different NH_4Cl concentrations. The plots for the O_2 release (τ_{O2}) are shown for the PSII fraction with fast O_2 formation (A) and for the PSII fraction with slow O_2 formation (B). In (A) and (B), average E_a-values are indicated, for individual E_a values see Table 1. The values for the time constant of O_2 formation, τ_{O2}, were obtained from simulation (fit) of the averaged O_2-transients of the 3rd to 14th flash applied to dark-adapted PSII. For each data point, the fit results of three experiments were averaged; the error bars indicate the corresponding standard deviations.

temperature in center of the investigated temperature range (here 20 °C).

The quantum yield of the tertiary light-driven reactions at the PSII donor side is lower than unity, largely due to charge recombination processes that compete with forward electron transfer [2,36]. This reduction in quantum yield (ϕ) can be viewed as resulting from 'miss events', which are described by the miss factor, m (ϕ = 100% - m); typical m-values for intact PSII range from 7 to 15% [9,10]. The miss events desynchronize cycling through the S-state cycle and thus result in deviations from the perfect flash number dependence with maximal O_2-yield on the 3rd, 7th, and 11th saturating flash of light applied to dark-adapted PSII. The extent of these deviations thus is informative regarding the miss-factor magnitude. Fig. 7 shows the flash-number dependence of the O_2 yield at 0°C and 30 °C for control-PSII without NH_4Cl (black curves) and with 100 mM NH_4Cl. Visual inspection facilitates an informative qualitative comparison of the miss-factor magnitude. Upon addition of 100 mM NH_4Cl, there is a fraction of Fast-PSII (orange curves) and Slow-PSII (blue curves), for which we determined the respective O_2-flash yield for each of the first 10 flashes individually, by simulation of the O_2 transients as described above. The control PSII (without NH_4Cl) exhibit a reasonably low miss factor at

Table 1
Time constants at 20 °C (τ_{O2}), the Arrhenius activation parameters (E_a and A, Eq. (1)) and Eyring's activation enthalpy and activation entropy ($\Delta H^{\ddagger}$ and $-T\Delta S^{\ddagger}$; Eqs. (2) and (3)). The values of $\Delta H^{\ddagger}$ and $T\Delta s$ are provided for 20 °C (293 K). The error ranges provided for E_a apply also for to the activation enthalpy and entropy.

	[NH_4Cl] (mM)	τ_{O2} (ms) at 20 °C	E_a (meV)	A (s^{-1})	$\Delta H^{\ddagger}$ (meV)	$-T\Delta S^{\ddagger}$ (meV)
Fast PSII fraction	0	1.71	241 ± 10	7.6×10^6	216	369
	20	1.82	258 ± 8	1.5×10^7	233	352
	60	1.74	244 ± 11	8.7×10^6	219	365
	100	1.69	248 ± 11	9.8×10^6	223	362
Slow PSII fraction	20	35.9	346 ± 12	2.2×10^7	321	342
	60	35.4	346 ± 14	2.2×10^7	321	342
	100	35.5	352 ± 13	2.9×10^7	327	335

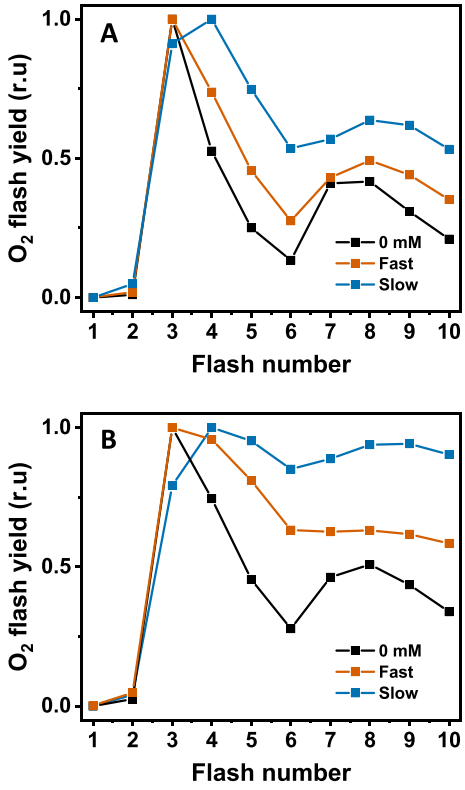

Fig. 7. Oxygen yield per flash for control PSII without NH_4Cl (black), Fast-PSII in the presence of 100 mM NH_4Cl (orange), and Slow-PSII in the presence of 100 mM NH_4Cl (blue). The O_2 transients were collected at 0 °C (A) and 30 °C (B). A sequence of saturating flashes of visible light (spaced by 900 ms) was applied to dark-adapted PSII. For each flash, the respective O_2-transient was recorded and analyzed. The shown O_2-flash-yield patterns are normalized to unity at the maximal O_2-yield. See also Fig. S6, for a complete temperature series.

0 °C (Fig. 7A), which is moderately increased at 30 °C (Fig. 7B). For the Fast-PSII, in the presence of NH_4Cl, we observe a significantly more pronounced de-synchronization (in comparison to the control PSII) indicative of an increased miss factor at both temperatures (strongly damped period-of-four oscillations) at both temperatures. For the Slow-PSII, the de-synchronization is increased further. Especially the increased miss factor of the Fast-PSII is informative. In the absence of any clear effect of NH_4Cl exposure on rate constant and activation energy of the O_2-formation step, the modified miss factor detected for the Fast-PSII fraction provides important support to NH_4^+/NH_3 binding to the Fast-PSII fraction.

4. Discussion

4.1. Three NH_4^+/NH_3 binding sites with distinctly different relations to the O_2-formation chemistry

Time-resolved detection of O_2 formation after light-flash excitation facilitated discrimination of NH_4^+/NH_3 binding at three sites resulting in three PSII fractions with distinct functional properties, in line with previous findings [24]. The K_m value for binding has been found to be around 20–30 mM (referring to the NH_4^+ concentration in the buffer solution) [24], without obvious differences in the K_m value when comparing the three sites. Also the data shown in Fig. 5 does not provide evidence for distinctly different K_m values, at least not in the temperature range from 5 °C to 30 °C, even though more minor differences cannot be excluded. We can only speculate on possible reasons for identical K_m values. Previously, we have suggested that identical K_m values could result from mutually exclusive, anti-cooperative NH_3 binding [24]. An alternative option is binding of NH_4^+/NH_3 in the S_1 state at a single binding site with a K_m value close to 25 mM followed by relocation in the S_2 state to different binding sites with similar affinities, possibly associated with NH_4^+ deprotonation and NH_3 binding to a manganese ion of the catalytic Mn_4CaO_5 cluster.

At largely saturating NH_4^+ concentration of 100 mM, we observe three PSII fractions distinguished by the following functional properties: (1) complete inhibition of O_2-formation, (2) fast O_2-formation with a time constant of 1.7 ms at 20 °C (Fast-PSII), and (3) slow O_2-formation with a time constant of 36 ms at 20 °C (Slow-PSII). For the Fast-PSII, we now determined an activation enthalpy of 223 ± 11 meV. Activation enthalpy and entropy of the Fast-PSII are essentially identical to the corresponding figures in the absence NH_4^+/NH_3 binding determined herein and elsewhere [32]. For the Slow-PSII, the activation enthalpy is 323 ± 11 meV and thus significantly increased, whereas the activation entropy remains essentially unchanged.

The completely unchanged properties of the O_2-formation step raises the question whether detection of the Fast-PSII fraction could result from an NH_4Cl concentration that was too low to allow for binding at all Slow-PSII and at all fully-inhibitory sites. However, the experimentally determined K_m values of 20–30 mM strongly suggest that NH_4^+/NH_3 binding at 100 mM NH_4Cl should be largely complete. In the present investigation, additional evidence for binding to the Fast-PSII fraction comes from the data of Fig. 7, which indicates that the Fast-PSII fraction at 100 mM NH_4Cl differs clearly in its miss factor from the PSII in NH_4Cl-free buffer. Thus we consider NH_4^+/NH_3 binding to the Fast-PSII fraction as likely and see two basic options to explain the unchanged properties of the O_2-formation step: Either (i) NH_4^+/NH_3 binding indeed occurs at a site without any influence on the O_2-formation step, excluding not only that the Fast-PSII site is a substrate-water site, but also any relevant modification of the H-bonded network formed by the water molecules, amino-acid residues and the nearby chloride ion. Or (ii) NH_4^+/NH_3 binding occurs in the S_2-state followed by unbinding before onset of the O—O bond formation step, in the $Y_Z{}^0S_3{}^+$ or $Y_Z{}^{ox}S_3{}^+$ or $Y_Z{}^{ox}S_3{}^n$ state. In line with the second option, the absence of bound ammonia in the S_3-state recently has been suggested based on EPR and kinetic UV–vis experiments [37]. We note that the second scenario does not exclude that in the S_2-state, the NH_4^+/NH_3 binding site of the Fast-PSII corresponds to a substrate-water site.

The fully inhibitory binding site could very well correspond to the binding site of a substrate-water molecule, whereas the lack of complete inhibition suggests that the Slow-PSII binding site is not identical with a water-binding site. We believe NH_4^+/NH_3 binding at the Slow-PSII site relates to disturbances of the H-bonded protein-water cluster(s) neighboring the Mn_4Ca-oxo core of the catalytic site. Evidence for this conjecture comes from comparison to genetic PSII variants. The time constant of the O_2-formation step in the Slow-PSII is 36 ms at 20 °C and thus very similar to time constants determined in mutants where the hydrogen-bonding network coupled to the Mn_4CaO_5 center was

modified by point mutations, e.g. D1-D61, D1-V185, D2-K317 and CP43-R357 [31,33–35]. However, here we find in the Slow-PSII a pronounced increase of the activation enthalpy, without major changes in the activation entropy (Table 1). In clear contrast, for PSII variants with severely retarded O_2-formation, a surprising decrease in activation enthalpy has been reported, which is overcompensated by less favorable entropic contribution to the total activation energy [35]. The clear increase in the activation enthalpy of the O_2-formation step implies that NH_4^+/NH_3 binding at the Slow-PSII site increases the energetic (enthalpic) barrier of the rate-determining step in O—O bond formation. The increased energetic barrier may be viewed as destabilization of the transition state or stabilization of an unfavorable active-site conformation before onset of the O—O bond formation step, where the active site comprises not only the catalytic metal-oxo complex and its first-sphere ligands, but also the surrounding protein-water environment.

4.2. Identification of the NH_4^+/NH_3 binding sites?

Previously, we suggested non-inhibitory ammonia binding to the water ligand of Mn4 denoted as W1 (see Fig. 1C) and inhibitory binding at the W2 site [24]. For these two sites, similar ammonia-binding energies are plausible as is mutually exclusive (anti-cooperative) binding, thereby explaining that a single K_m value that describes the formation of an inhibited PSII fraction and an uninhibited PSII fraction. FTIR S-state difference spectra indicated that the uninhibited PSII fraction is associated with spectral changes that exhibit clear similarities to spectral changes observed for mutation of the D61 residue (of the D1 protein of PSII), which is an H-bonding partner of W1, thereby providing support to assignment of the non-inhibitory ammonia-binding site to W1. However, similar spectral changes are also observed for other genetic modifications that affect the H-bonded protein-water network surrounding W1 and W2. On these grounds, also non-inhibitory binding at different sites in vicinity of W1 cannot be excluded. A recent computational investigation evaluated six putative binding positions in the second coordination sphere of the Mn_4Ca-oxo cluster. Two of these were judged as being of possible relevance; one involves the NH_4^+-$K317^0$-$D61^-$ ion pairing [38].

Our suggestion of non-inhibitory binding at the W1 site [24] was motivated by experimental evidence obtained by means of advanced EPR investigations on PSII in its S_2-state combined with detection of substrate-water exchange rates and computational methods [39]. Ammonia binding to Mn4 with strong H-bond to D61 was later confirmed by other investigators [40]. It was concluded that non-inhibitory ammonia binding occurs at the W1 site of PSII, thereby rendering a role of W1 as a substrate-water molecule unlikely [39]. Although not necessarily in conflict with this conclusion, our results suggest that also other scenarios are conceivable that do *not* exclude W1 as a substrate water molecule:

(1) There exists a fully inhibitory NH_4^+/NH_3 binding site which could relate to bound NH_3 replacing one of the two substrate-water molecules. Here ammonia might replace the W2 ligand of Mn4 (Fig. 1C), but solid evidence for this conjecture is still lacking.
(2) There exists a NH_4^+/NH_3 binding site, for which the average quantum yield of the S-state transitions is significantly lowered (higher miss factor) but the kinetics of the O_2-formation steps are not at all affected (unchanged activation enthalpy and entropy). This binding site could correspond to the W1 ligand of Mn4 (Fig. 1C). However, it is unlikely that ammonia still bound at the W1 site in the O_2-formation step (and thus affecting the surrounding H-bond network) would leave the kinetic characteristics completely unaffected. To explain fully non-inhibitory ammonia binding at the W1 site, we tentatively propose that NH_3/NH_4^+ binding in the S_2-state of PSII is followed by unbinding before onset of the O—O bond formation step. This scenario is not easily reconciled with the carousel mechanism [22,26]. It implies that assignment of W1 to a substrate-water molecule can *not* be ruled out (in contrast to a conclusion in [39]). We note that, based on DFT calculations, recently Siegbahn ruled out pivot or carousel mechanisms because the involved 5-coordinated Mn(IV) complex would be too high in energy [41].
(3) There exists a site where NH_3/NH_4^+ binding increases the energetic barrier of the O—O bond formation step significantly. This site is not a substrate-water site. It likely is within the H-bonded protein-water cluster in vicinity of the Mn_4Ca-oxo cluster that comprises also W1 and W2. Binding by replacement of W1 or W2 cannot be excluded, but we consider a location outside the first coordination sphere of Mn4 as being more likely.

Transparency document

The Transparency document associated this article can be found, in online version.

Acknowledgements

We thank Philipp Simon and Zhiyong Liang for experimental support; we acknowledge stimulating discussion with Paul Greife, Nils Schuth, and Michael Haumann (all at Freie Univ. Berlin). We gratefully acknowledge financial support by Deutsche Forschungsgemeinschaft (DFG) to the SFB 1078, a collaborative research center on protonation dynamics in protein function (project A4-Dau).

Appendix A. Supplementary data

Supplementary data to this article can be found online at https://doi.org/10.1016/j.dummy.2019.01.002.

References

[1] G. Renger, T. Renger, Photosystem II: the machinery of photosynthetic water splitting, Photosynth. Res. 98 (2008) 53–80.
[2] H. Dau, I. Zaharieva, Principles, efficiency, and blueprint character of solar-energy conversion in photosynthetic water oxidation, Acc. Chem. Res. 42 (2009) 1861–1870.
[3] R.E. Blankenship, Molecular Mechanisms of Photosynthesis, Blackwell Science, England, Oxford, 2002.
[4] I. Zaharieva, M.M. Najafpour, M. Wiechen, M. Haumann, P. Kurz, H. Dau, Synthetic manganese-calcium oxides mimic the water-oxidizing complex of photosynthesis functionally and structurally, Energy Environ. Sci. 4 (2011) 2400–2408.
[5] C.X. Zhang, C.H. Chen, H.X. Dong, J.R. Shen, H. Dau, J.Q. Zhao, A synthetic Mn_4Ca-cluster mimicking the oxygen-evolving center of photosynthesis, Science 348 (2015) 690–693.
[6] H. Dau, M. Haumann, The manganese complex of photosystem II in its reaction cycle—basic framework and possible realization at the atomic level, Coord. Chem. Rev. 252 (2008) 273–295.
[7] W. Junge, M. Haumann, R. Ahlbrink, A. Mulkidjanian, J. Clausen, Electrostatics and proton transfer in photosynthetic water oxidation, Philos. Trans. R. Soc. B 357 (2002) 1407–1418.
[8] H. Dau, M. Haumann, Eight steps preceding O-O bond formation in oxygenic photosynthesis—a basic reaction cycle of the photosystem II manganese complex, Biochim. Biophys. Acta 1767 (2007) 472–483.
[9] B. Kok, B. Forbush, M. McGloin, Cooperation of charges in photosynthetic O_2 evolution - I. A linear four-step mechanism, Photochem. Photobiol. 11 (1970) 457–475.
[10] H. Dau, M. Haumann, Time-resolved X-ray spectroscopy leads to an extension of the classical S-state cycle model of photosynthetic oxygen evolution, Photosynth. Res. 92 (2007) 327–343.
[11] A. Klauss, M. Haumann, H. Dau, Alternating electron and proton transfer steps in photosynthetic water oxidation, Proc. Natl. Acad. Sci. U. S. A. 109 (2012) 16035–16040.
[12] M. Haumann, P. Liebisch, C. Muller, M. Barra, M. Grabolle, H. Dau, Photosynthetic O_2 formation tracked by time-resolved x-ray experiments, Science 310 (2005) 1019–1021.
[13] Y. Umena, K. Kawakami, J.-R. Shen, N. Kamiya, Crystal structure of oxygen-evolving photosystem II at a resolution of 1.9 Å, Nature 473 (2011) 55–60.
[14] M. Suga, F. Akita, K. Hirata, G. Ueno, H. Murakami, Y. Nakajima, T. Shimizu, K. Yamashita, M. Yamamoto, H. Ago, J.-R. Shen, Native structure of photosystem II at 1.95 Å resolution viewed by femtosecond X-ray pulses, Nature 517 (2015) 99–103.

[15] M. Retegan, F. Neese, D.A. Pantazis, Convergence of QM/MM and cluster models for the spectroscopic properties of the oxygen-evolving complex in photosystem II, J. Chem. Theory Comput. 9 (2013) 3832–3842.
[16] P.E.M. Siegbahn, Water oxidation mechanism in photosystem II, including oxidations, proton release pathways, O—O bond formation and O_2 release, Biochim. Biophys. Acta 1827 (2013) 1003–1019.
[17] E.M. Sproviero, J.A. Gascón, J.P. McEvoy, G.W. Brudvig, V.S. Batista, QM/MM models of the O_2-evolving complex of photosystem II, J. Chem. Theory Comput. 2 (2006) 1119–1134.
[18] P.E. Siegbahn, A structure-consistent mechanism for dioxygen formation in photosystem II, Chem. Eur. J. 14 (2008) 8290–8302.
[19] P.E.M. Siegbahn, Nucleophilic water attack is not a possible mechanism for O-O bond formation in photosystem II, Proc. Natl. Acad. Sci. U. S. A. 114 (2017) 4966–4968.
[20] D. Narzi, M. Capone, D. Bovi, L. Guidoni, Evolution from S_3 to S_4 state of the oxygen evolving complex in Photosystem II monitored by QM/MM dynamics, Chem. Eur. J. 24 (2018) 10820–10828.
[21] D.A. Pantazis, Missing pieces in the puzzle of biological water oxidation, ACS Catal. 8 (2018) 9477–9507.
[22] M. Askerka, G.W. Brudvig, V.S. Batista, The O_2-evolving complex of photosystem II: recent insights from quantum mechanics/molecular mechanics (QM/MM), extended X-ray absorption fine structure (EXAFS), and femtosecond X-ray crystallography data, Acc. Chem. Res. 50 (2017) 41–48.
[23] N. Cox, J. Messinger, Reflections on substrate water and dioxygen formation, Biochim. Biophys. Acta 1827 (2013) 1020–1030.
[24] N. Schuth, Z. Liang, M. Schonborn, A. Kussicke, R. Assuncao, I. Zaharieva, Y. Zilliges, H. Dau, Inhibitory and non-inhibitory NH_3 binding at the water-oxidizing manganese complex of photosystem II suggests possible sites and a rearrangement mode of substrate water molecules, Biochemistry 56 (2017) 6240–6256.
[25] A. Boussac, A.W. Rutherford, S. Styring, Interaction of ammonia with the water splitting enzyme of photosystem II, Biochemistry 29 (1990) 24–32.
[26] D.J. Vinyard, M. Askerka, R.J. Debus, V.S. Batista, G.W. Brudvig, Ammonia binding in the second coordination sphere of the oxygen-evolving complex of photosystem II, Biochemistry 55 (2016) 4432–4436.
[27] R.G. Mortimer, H. Eyring, Elementary transition-state theory of the Soret and Dufour effects, Proc. Natl. Acad. Sci. U. S. A. 77 (1980) 1728–1731.
[28] H. Schiller, H. Dau, Preparation protocols for high-activity photosystem II membrane particles of green algae and higher plants, pH dependence of oxygen evolution and comparison of the S_2-state multiline signal by X-band EPR spectroscopy, J. Photochem. Photobiol. B 55 (2000) 138–144.
[29] A.R. Wellburn, The spectral determination of chlorophylls a and b, as well as total carotenoids, using various solvents with spectrophotometers of different resolution, J. Plant Physiol. 144 (1994) 307–313.
[30] L.C. Clark, R. Wolf, D. Granger, Z. Taylor, Continuous recording of blood oxygen tensions by polarography, J. Appl. Physiol. 6 (1953) 189–193.
[31] P.L. Dilbeck, H.J. Hwang, I. Zaharieva, L. Gerencser, H. Dau, R.L. Burnap, The mutation D1-D61N in Synechocystis sp. PCC 6803 allows the observation of pH-sensitive intermediates in the formation and release of O_2 from Photosystem II, Biochemistry 51 (2012) 1079–1091.
[32] J. Buchta, M. Grabolle, H. Dau, Photosynthetic dioxygen formation studied by time-resolved delayed fluorescence measurements—method, rationale, and results on the activation energy of dioxygen formation, Biochim. Biophys. Acta 1767 (2007) 565–574.
[33] H.J. Hwang, P. Dilbeck, R.J. Debus, R.L. Burnap, Mutation of arginine 357 of the CP43 protein of photosystem II severely impairs the catalytic S-state cycle of the H2O oxidation complex, Biochemistry 46 (2007) 11987–11997.
[34] R. Pokhrel, R.J. Service, R.J. Debus, G.W. Brudvig, Mutation of lysine 317 in the D2 subunit of Photosystem II alters chloride binding and proton transport, Biochemistry 52 (2013) 4758–4773.
[35] H. Bao, R.L. Burnap, Structural rearrangements preceding dioxygen formation by the water oxidation complex of photosystem II, Proc. Natl. Acad. Sci. U. S. A. 112 (2015) E6139–E6147.
[36] M. Grabolle, H. Dau, Efficiency and role of loss processes in light-driven water oxidation by PSII, Physiol. Plant. 131 (2007) 50–63.
[37] A. Boussac, I. Ugur, A. Marion, M. Sugiura, V.R. Kaila, A.W. Rutherford, The low spin-high spin equilibrium in the S_2-state of the water oxidizing enzyme, Biochim. Biophys. Acta 1859 (2018) 342–356.
[38] M. Mandal, M. Askerka, G. Banerjee, M. Amin, G.W. Brudvig, V.S. Batista, M. Gunner, Characterization of ammonia binding to the second coordination shell of the oxygen-evolving complex of photosystem II, Dalton Trans. 46 (2017) 16089–16095.
[39] M.P. Navarro, W.M. Ames, H. Nilsson, T. Lohmiller, D.A. Pantazis, L. Rapatskiy, M.M. Nowaczyk, F. Neese, A. Boussac, J. Messinger, W. Lubitz, N. Cox, Ammonia binding to the oxygen-evolving complex of photosystem II identifies the solvent-exchangeable oxygen bridge (μ-oxo) of the manganese tetramer, Proc. Natl. Acad. Sci. U. S. A. 110 (2013) 15561–15566.
[40] P.H. Oyala, T.A. Stich, R.J. Debus, R.D. Britt, Ammonia binds to the dangler manganese of the photosystem II oxygen-evolving complex, J. Am. Chem. Soc. 137 (2015) 8829–8837.
[41] P.E.M. Siegbahn, The S_2 to S_3 transition for water oxidation in PSII (photosystem II), revisited, Phys. Chem. Chem. Phys. 20 (2018) 22926–22931.